https://doi.org/10.1007/s41230-022-2048-4

Fabrication of silica-based ceramic cores with internal lattice structures by stereolithography

Ke-hui Hu[1, 2], Hao-yuan Wang[1, 2], Kuan Lu[3], Qian Feng[1, 2], Dao-ding Yang[4], Jian Cao[4], Bo Zhang[4], *Zhi-gang Lü[1, 2, 5], and **Xing Ran[2, 4]

1. State Key Laboratory of Tribology, Tsinghua University, Beijing 100084, China

2. Department of Mechanical Engineering, Tsinghua University, Beijing 100084, China

3. Ten Dimensions (Guangdong) Technology Co., Ltd., Foshan 528225, Guangdong, China

4. Guizhou Anji Aviation Investment Casting Co., Ltd., Anshun 561003, Guizhou, China

5. Key Laboratory of Advanced Materials Processing Technology, Ministry of Education, Tsinghua University, Beijing 100084, China

Abstract: Ceramic cores are widely used in investment casting, and ideal properties of cores are essential for high-quality castings. Under the circumstances requiring thick cores, solid cores are likely to encounter deformation and cracking defects due to the accumulation of shrinkage. Therefore, with the superiority of ceramic stereolithography in producing complex ceramic parts, hollow cores with lattice structures were designed and fabricated. The dimensional accuracy and properties of the green and sintered bodies were evaluated. Results show the dimensional accuracy of sintered cores is controlled within ±0.25 mm benefited from the precise green bodies. The mechanical properties are not obviously deteriorated. The bending strength reaches 11.94 MPa at room temperature and 12.87 MPa at 1,500 °C with a creep deformation of 0.345 mm. Furthermore, casting verifications prove that the hollow cores meet the requirements of investment casting. Smooth casting surfaces are obtained, at the same time, the core-removal efficiency is improved by over 3 times.

Keywords: silica; ceramic cores; stereolithography; lattice structure; investment casting

CLC numbers: TG221 **Document code:** A **Article ID:** 1672-6421(2022)05-369-11

1 Introduction

Ceramic cores are crucial to the forming of cavity features in investment casting. For example, the casting of the gas-turbine blades with internal cooling canals involves ceramic cores throughout the entire process [1]. To successfully cast the cavities, the properties of ceramic cores should meet the following requirements [2]:

(1) High mechanical strength at room temperature to withstand the impact of high-speed flow during the wax injection process.

(2) Moderate high-temperature strength and superior creep resistance to withstand the mechanical and thermal shock of molten metals during the pouring process while ensuring deformability during the solidifying stage.

(3) Adequate thermochemical stability when in contact with reactive metals at high temperature.

(4) High dimensional accuracy to ensure the dimensional accuracy of castings.

(5) Low surface roughness for high casting surface quality.

(6) Compatible porosity and chemical reactivity to efficiently remove cores without damaging castings.

The injection moulding method is typically used for the fabrication of ceramic cores [3]. However, this manufacturing method involves moulds which can impose limitations on core complexity. Furthermore, for the castings requiring thick cores, solid cores perform poorly in heat conduction, which not only increases the difficulty of core removal but also deteriorates the forming quality of castings and leads to deformation and cracking defects.

The limitations of conventional forming methods can be improved through additive manufacturing (AM) approaches. 3D printing and layered extrusion forming techniques have been applied in the fabrication of complex-shaped cores of calcia-based and alumina-based ceramics [4-7]. High-performance silica-based cores have also been fabricated by selective laser

***Zhi-gang Lü**

Born in 1972, Ph.D, Professor. His research interests mainly focus on investment casting and additive manufacturing of ceramic materials.

E-mail: lvzg@tsinghua.edu.cn

****Xing Ran**

E-mail: ranxing257@163.com

Authors Ke-hui Hu and Hao-yuan Wang contributed equally to this article.

Received: 2022-04-01; Accepted: 2022-07-24

sintering combined with vacuum infiltration process [8]. In addition to these approaches, ceramic stereolithography, a photo-curing AM method, has rapidly progressed in recent years [9]. The basic principle of this method is to mix the photo-curable resin and ceramic powders and then form the suspensions into green parts with stereolithography devices [10, 11]. With further postprocessing including binder removal and sintering, dense ceramic components are obtained with ideal properties [12, 13]. Compared with other AM techniques that can also be applied to ceramics, ceramic stereolithography provides superior mechanical strength and low surface roughness [14].

Ceramic stereolithography has been applied to fabricate ceramic cores and shells in investment casting [15-18]. Silica ceramic cores and integrally cored ceramic moulds were built by ceramic stereolithography, and practical casting verifications have been successfully carried out for single-crystal blades [16, 17]. Furthermore, more complex ceramic core over 120 mm in height were manufactured by ceramic stereolithography [18]. Both the mechanical strength and forming accuracy could meet the requirements of single-crystal investment castings. A summary of the typical properties of the silica-based ceramic cores is given in Table 1. It can be concluded that there is no obvious difference in the apparent porosity, while the cores fabricated by ceramic stereolithography have poorer mechanical performance and higher sintering shrinkage. However, casting verifications have proven the qualification of stereolithography-fabricated cores for investment casting and the high sintering shrinkage can be compensated for by enlarging the size of the digital model. Compared with the injection moulding method, ceramic stereolithography brings more benefits including complex structural design and a shortened production cycle due to elimination of moulds.

Table 1: Typical properties of the silica-based ceramic cores. For the cores built by stereolithography, sintering shrinkages vary in the build direction (*Z* direction) and in the projection plane (*X*-*Y* plane). Sintering temperatures corresponding to the shrinkages are also specified

Reference	Year	Process	Sintering shrinkage (%)	Apparent porosity (%)	Bending strength (MPa)	Creep deformation (mm)
Xu et al. [19]	2019	Injection moulding with 0.6wt.% addition of silica nanopowders	0.6 (1,190 °C)	27.5	30.5	0.2
Niu et al. [20]	2020	Injection moulding with reinforcement of mullite fibres	0.8 (1,190 °C)	35.2	25.5	0.12
Hu et al. [18]	2021	Stereolithography	4.2 (*X*-*Y*) / 6.0 (*Z*) (1,200 °C)	28.2	18.4	\
Li et al. [21]	2021	Stereolithography	2.9 (*X*-*Y*) / 4.6 (*Z*) (1,200 °C)	35.1	9.1	\
Wang et al. [22]	2021	Stereolithography with 0.5wt.% addition of silica nanopowders	3.6 (*X*-*Y*) / 4.6 (*Z*) (1,200 °C)	34.0	6.6	0.35

By applying ceramic stereolithography, complex cellular ceramics with lattice structures can be produced [23-26]. In previous studies, different lattice configurations were designed and tested to obtain the optimized mechanical behaviors [27-29]. Furthermore, since heat is released during the polymerization of ceramic suspensions with volume shrinkage, it was also found that the accumulation of shrinkage exists as one of the main factors causing the deformation and cracking of the stereolithography-fabricated ceramic parts [30, 31]. Therefore, by reducing the volume and therefore lowering the released heat, the lattice structure helps to reduce the shrinkage stress while maintaining the necessary mechanical strength. In addition, the porous architecture also promotes the evacuation of the gases generated during the binder removal and thus avoids the formation of cracks caused by the rise of inner pressure [32]. The lattice structures can help avoid the problems encountered by solid cores while there has been no report on the combination of ceramic cores and lattice structures.

In this work, to improve the forming quality of the silica-based ceramic cores for investment casting, hollow cores with lattice structures inside were designed and fabricated using ceramic stereolithography. The dimensional accuracy and properties of the green and sintered bodies were evaluated. Furthermore, practical casting processes using the hollow cores were carried out to verify the qualification for investment casting.

2 Experimental procedures

2.1 Materials

The materials used to fabricate the ceramic cores are composed of fused silica, zirconium silicate, and alumina in a weight proportion of 14:4:1. The corresponding mass fractions as well as the particle sizes are listed in Table 2. Figure 1 presents the microstructures of the powders. The ceramic powders were first mechanically mixed with the photo-curable resin (Ten Dimensions Tech. Co., Ltd., 10D-S-02). Then, the mixture was ball milled for 12 h to obtain uniformly distributed suspensions. Final suspensions for stereolithography were prepared after

Table 2: Composition of the ceramic powders

Material	Chemical formula	Fraction (wt.%)	Density ($g \cdot cm^{-3}$)	Purity (%)	Particle size (μm)			Producer
					D (10)	*D* (50)	*D* (90)	
Fused silica	SiO_2	73.684	2.21	> 98	1.176	5.639	24.415	Ten Dimensions Tech. Co., Ltd.
Zirconium silicate	$ZrSiO_4$	21.053	3.96	(ZrO_2) 65.5	0.434	0.984	1.972	Kinsei Matec Co., Ltd.
Alumina	Al_2O_3	5.263	4.56	> 99.8	2.490	7.829	18.125	Aluminum Co., of China Ltd.

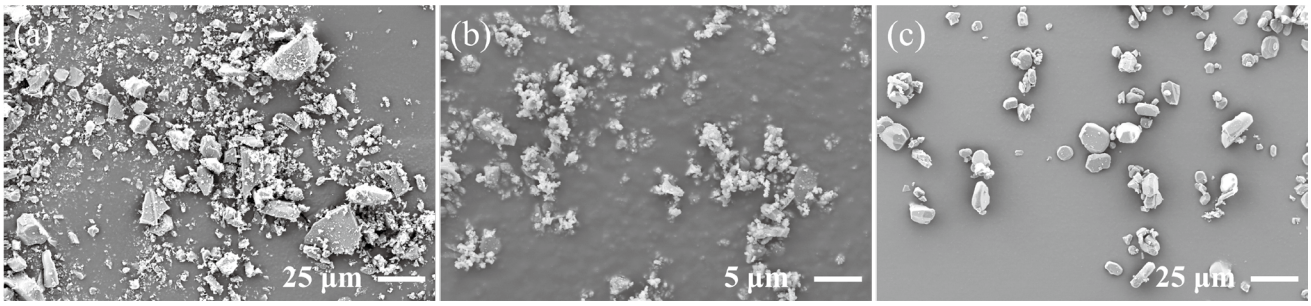

Fig. 1: Microstructures of the component materials of the ceramic powders: (a) fused silica; (b) zirconium silicate; (c) alumina

vacuum deaeration for 30 min and standing for 2 h. The solid content of the prepared suspensions was 58vol.%. The viscosity was 10.8 Pa·s at 25 °C and 100 s^{-1}.

2.2 Design of ceramic cores

A hollow design was adopted for the cores. Therefore, the internal structure to support the hollow cavity was firstly determined. Different lattice structures were tested and compared, including body diagonals, octet truss, cross cube 14 (with a relative density of 14%), and cross cube 33 (with a relative density of 33%). As the cores are required to withstand the impact during different processes of investment casting, the compressive strengths of these structures were tested with cylinder specimens, and each structure was tested with 4 specimens. Figure 2 presents these ceramic specimens and the corresponding unit cells, where the specimens were 40 mm in diameter and 19 mm in height. The unit cell lengths varied from 4.0 mm to 4.8 mm. The testing results of the compressive strengths and the relative densities are shown in Table 3. It should be noted that the relative densities were measured by comparing the volumes of the hollow specimens with the solid specimen, and each structure was tested with 4 specimens.

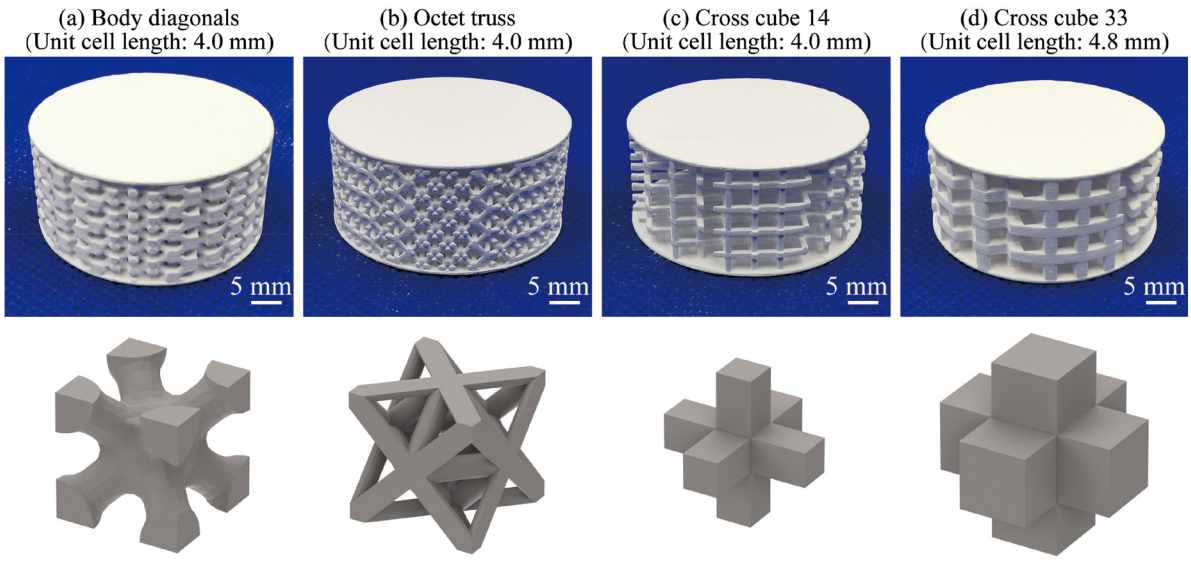

Fig. 2: Ceramic specimens with lattice structures for compressive strength testing and the corresponding unit cells: (a) body diagonals; (b) octet truss; (c) cross cube 14 (with a relative density of 14%); (d) cross cube 33 (with a relative density of 33%)

Therefore, as the specimens were cylinders with incomplete cells, the relative densities can slightly deviate from the theoretical values of the corresponding unit cells. Then, the normalized compressive strengths were calculated considering the relative densities. It can be concluded that the cross cube 33 shows the best compressive performance and was chosen as the lattice structure to support the hollow cores.

Furthermore, the main body of the ceramic cores is in the shape of a plate. Figure 3(a) presents the computer-aided design (CAD) model of the cores showing the external shape. The outline dimensions are 108 mm×50 mm×24 mm. At the upper surface and two ends of the core, locating characteristics were designed.

With the desired external shape and the internal cavity, the hollow core was finally designed. The wall thickness was 2 mm, and the internal lattice structure adopted the cross cube unit cell with the unit length of 4.8 mm and the relative density of 33%. Figures 3(b) and (c) present the complete structure of the core and its slices respectively, showing the internal cavity supported by the lattice structure.

Table 3: Relative densities and compressive strengths of the lattice structures

Lattice structure	Relative density (%)	Compressive strength (MPa)	Compressive strength normalized by relative density (MPa)
Body diagonals	48	7.16 ± 0.37	14.92
Octet truss	33	3.18 ± 0.52	9.64
Cross cube 14	14	1.60 ± 0.28	11.43
Cross cube 33	33	8.36 ± 0.33	25.33

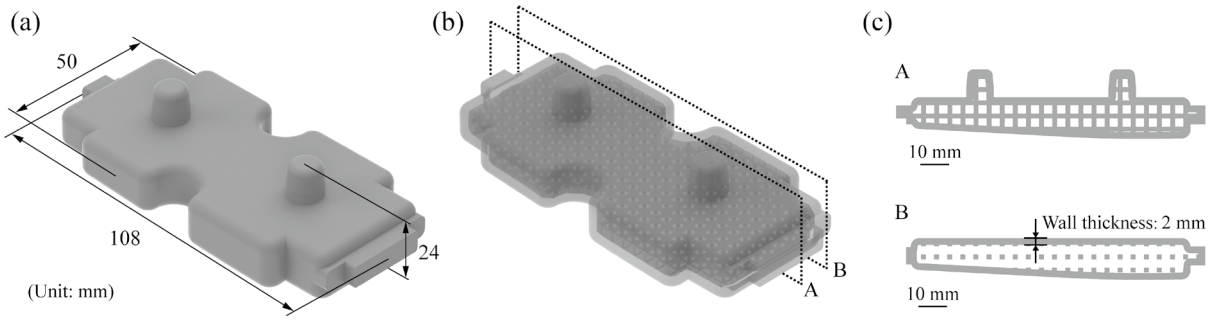

Fig. 3: CAD model of the hollow ceramic cores: (a) external shape; (b) complete structure; (c) slices

2.3 Fabrication of ceramic cores

The ceramic cores were fabricated using the ceramic stereolithography method. Figure 4(a) presents the diagram of the adopted stereolithography apparatus (Ten Dimensions Tech. Co., Ltd., AutoCera-L). The light is projected from the bottom and solidifies the suspensions as the build platform continuously moves upwards for new layers to be generated based on the previous layers. The digital light processing (DLP) projector equipped in the device can achieve a resolution of 35 μm within the projection plane (*X*-*Y* plane). With the repeated positioning precision of 2 μm in the build direction (*Z* direction), the maximum dimensions of the fabricated objects can reach 136 mm×76 mm×200 mm.

With a preliminary study on stereolithography-fabricated ceramic cores, a layer thickness of 50 μm had been found to balance the dimensional accuracy and production efficiency and therefore was adopted [18]. To determine the photo-curing parameters corresponding to the slice thickness, a series of tests were carried out relating to the relationship between the light exposure and the cured layer. As Fig. 4(b) shows, as UV light was projected onto the suspensions forming a cured layer with the desired width, excess cure areas were also solidified beyond the range of projection. Then, after cleaning the residual suspensions, the cure depth C_d and the excess cure width W_{ex} were measured through a thickness meter and an optical microscope, respectively. The incident energy E_0, a combination of light intensity W and exposure time t, was measured by a radiometer (Linshang Tech. Co., Ltd., LS125-E395).

It was assumed that both the cure depth and the excess cure width follow the Beer-Lambert absorption relationship [9, 33]:

$$C_d = S_d \ln(E_0/E_c) \quad (1)$$

$$W_{ex} = S_w \ln(E_0/E_w) \quad (2)$$

where S_d is the depth sensitivity that is defined as the magnitude of the attenuation length. The depth critical energy E_c is the minimum energy needed to initiate the reaction. At the cure depth, the polymerization reaction reaches the gel point with the critical energy. The width sensitivity S_w and the width critical energy E_w are the corresponding parameters in the horizontal direction. Then, as Fig. 5 shows, the testing results

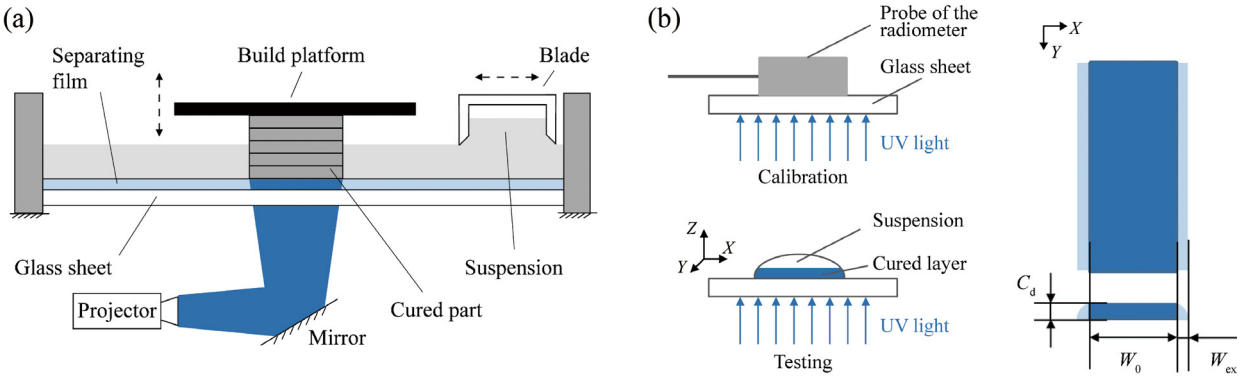

Fig. 4: Diagrams of the stereolithography process: (a) schematic diagram of the stereolithography apparatus; (b) measurement of cure depth C_d and the excess cure width W_{ex} with corresponding incident energy E_0

were fitted by the relationship in Eq. (1) and Eq. (2) using the least-squares method. Previous research has found that a higher cure depth is beneficial to improving interlayer bonding and reducing cracks in sintered bodies [34]. However, to realize higher cure depth, larger excess cure width is inevitable with more incident energy. To balance the interlayer bonding strength and the dimensional accuracy, an incident energy of 300 mJ·cm^{-2} was chosen with a cure depth of 173 μm. Table 4 summarizes the process parameters used for fabricating the ceramic cores. The incident energy was controlled by taking the light intensity of 30 mW·cm^{-2} and exposure time of 10 s. In addition, based on the fitting results, the excess cure width corresponding to the chosen incident energy was 200 μm. The obtained excess cure width was further used for the compensations described in Section 3.1.

After the photo-curing process, to evaluate the dimensional accuracy, the green bodies of the cores were scanned using a blue light three-dimensional scanner (SHINING 3D Tech. Co., Ltd., OptimScan-5M). Then, the stereolithography-fabricated green bodies were processed through the temperature system presented in Fig. 6 to remove the binder and sinter the ceramics, which was determined through a thermogravimetric analysis [18]. Sintering was completed at 1,200 °C for 2 h.

Table 4: Stereolithography process parameters

Parameter	Value
Slice thickness δ_0	50 μm
Light intensity W	30 mW·cm^{-2}
Exposure time t	10 s
Cure depth C_d	173 μm
Excess cure width W_{ex}	200 μm

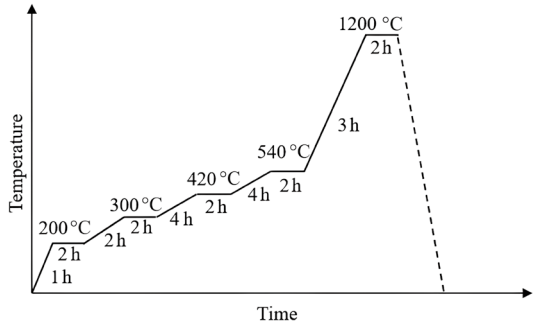

Fig. 6: Temperature system for binder removal and sintering of the ceramic core

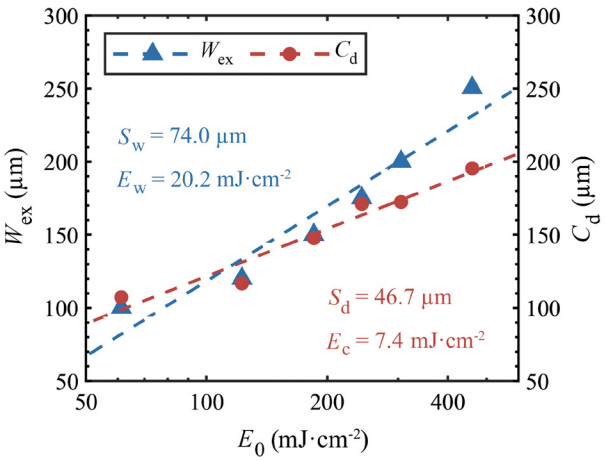

Fig. 5: Cure depth C_d and excess cure width W_{ex} versus incident energy E_0. The scale of the incident energy is in logarithmic terms. The fitting results of Eq. (1) and Eq. (2) are also presented

2.4 Casting verification

After the fabrication of ceramic cores, practical castings using the cores were produced to verify if the cores could meet the requirements of investment casting. The pouring metal of the castings was the nickel-based superalloy K4648. Before casting, the assembled moulds with the cores inside were roasted at 1,050 °C for 2–3 h, where the heating stage from the room temperature was at the heating rate of 8.75 °C·min^{-1}. Then, the casting process including preheating, pouring, and cooling was conducted. Firstly, the moulds were preheated at 1,050 °C for 8–15 h. After that, the moulds were transferred to a vacuum furnace for pouring. The molten metal was heated to 1,550 °C and then poured into the moulds. Finally, when the temperature dropped to 100–150 °C, the moulds and the castings proceeded to the subsequent mould removal processes. The cores were removed by soaking in a 50wt.% solution of potassium hydroxide (KOH) at 160 °C and 0.6 MPa.

3 Results and discussion

3.1 Dimensional accuracy of green bodies

Figure 7 presents the green bodies with lattice structures fabricated by ceramic stereolithography that are smooth and free of defects on the surfaces. The internal lattice structure is completely shaped.

For the fabrication of the green bodies, two issues were considered, including the error led by the excess cure width and the effect of part orientation. As stated in Section 2.3, with the suspensions and the photo-curing parameters taken in the stereolithography process, the excess cure width in this study reaches 200 μm. When directly fabricating the green bodies with the design model, large dimensional errors were obtained, as shown in Fig. 8(a). Due to the excess cure width, the whole core is oversized and out of tolerance. Therefore, compensations for the excess cure width were made. Figure 8(b) presents the diagram of the compensations, which were completed on the slices of the design model. At the edges of the slices, areas with a constant width equal to the excess cure width were subtracted. In other words, with the grey areas as the original design, the red areas were subtracted, and the blue areas were finally sent to the stereolithography apparatus for fabrication. Then, the compensated green bodies could achieve higher dimensional accuracy, as shown in Fig. 9 and Fig. 10.

Furthermore, anisotropic properties are inevitable for the parts manufactured by ceramic stereolithography because of the layer-by-layer building process. Therefore, two part orientations were tested and compared, which are parallel to and perpendicular to the build direction, respectively, as shown in Fig. 7(a) and Fig. 7(b). The build platform can arrange three cores adopting the vertical orientation (parallel to the build direction) or one adopting the horizontal orientation (parallel to the build direction).

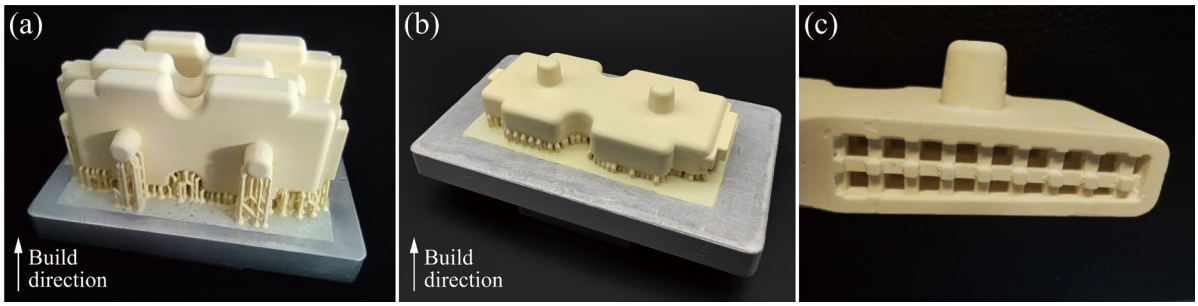

Fig. 7: Green bodies of the ceramic cores fabricated using ceramic stereolithography: (a) three cores arranged on the build platform adopting the vertical orientation (parallel to the build direction); (b) one core on the build platform adopting the horizontal orientation (perpendicular to the build direction); (c) a half-finished sample showing inside lattice structure

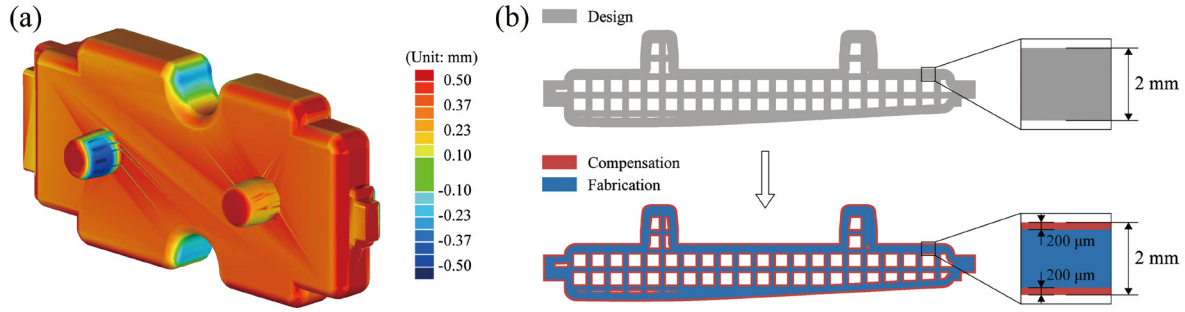

Fig. 8: Dimensional errors led by the excess cure width and the corresponding compensations: (a) difference between the design model and the green body sample fabricated without compensations and adopted the vertical orientation; (b) diagram of the compensations for the excess cure width made on the slices of the core

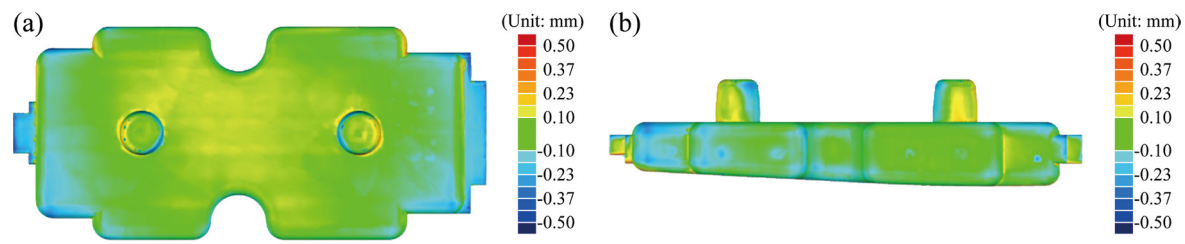

Fig. 9: Difference between the design model and the green body sample fabricated with compensation and adopting the vertical orientation: (a) top view; (b) side view

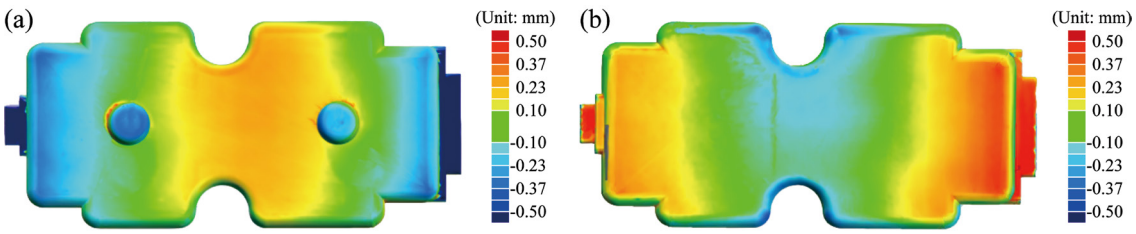

Fig. 10: Difference between the design model and the green body sample fabricated with compensation and adopting the horizontal orientation: (a) top view; (b) bottom view

The core adopting the vertical orientation reaches a stable and ideal difference all over the part within ±0.25 mm. While, severe warped deformations occur to the horizontal one at the two ends of the core, where the maximum difference reaches 0.5 mm. This can be attributed to the large cross-sectional area of the horizontal orientation that causes more shrinkage. The sample by vertical orientation with fewer suspensions cured at the same time can be less affected by the shrinkage. In addition, the vertical orientation enables more cores to be fabricated at the same time with the limited build platform and increases the production efficiency. Therefore, the vertical orientation is chosen for the manufacturing of the green bodies to proceed to the subsequent sintering process. The advantage of the reduced cross-sectional area also suggests the superiority of the lattice structure compared with the solid structure in improving the dimensional accuracy of the green bodies.

3.2 Dimensional accuracy and properties of sintered bodies

During the sintering process, the accumulation of the stress led by sintering shrinkage can lead to cracks. In addition, the release of a great amount of gas produced during binder removal can also result in the rise of inner pressure and therefore the formation of cracks. Figure 11 presents a practical solid core that cracked after binder removal and sintering. One long crack appears at the interlayer bonding, and more cracks occur within the projection plane (*X*-*Y* plane). The former crack might be attributed to weak interlayer bonding, the latter cracks are more related to shrinkage stress and gas evacuation. Therefore, the hollow design with the lattice structure is necessary to avoid such cracks while maintaining mechanical strength.

A hollow ceramic core sample after sintering is shown in Fig. 12(a). The external shape of the core is complete without cracks. A high surface finish was achieved on the sintered bodies as on the green bodies. Figure 12(b) presents the hollow cavity supported by the lattice structure. The lattice structure retains its structural integrity after sintering. The improvements brought by the hollow design can be attributed to a larger space for the evacuation of the gas generated during binder removal, and less accumulation of the shrinkage stress.

In addition, stereolithography-fabricated cores generally shrink by approximately 5% during sintering, which is nonneglectable. Therefore, compensations were also made with the premeasured shrinkage. The cores were compensated for by enlarging the original three-dimensional model by 4.60% in the build direction (*Z* direction) and 3.14% in the projection plane (*X*-*Y* plane). It should be noted that the compensations for the sintering shrinkage and excess cure width were different and sequentially made. As the cores were firstly cured and then sintered, the design model of the cores was first entirely enlarged compensating for the shrinkage and then subtracted in each slice compensating for the excess cure width. The green bodies and the sintered bodies were compared with the corresponding models.

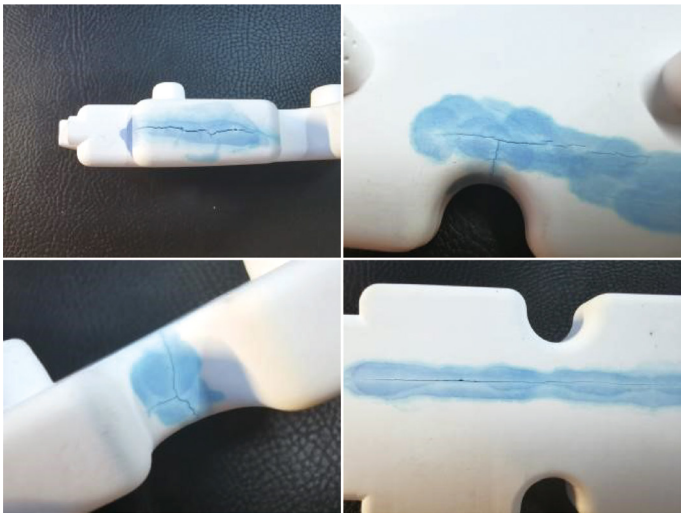

Fig. 11: Cracks of the solid core sample occurring during sintering

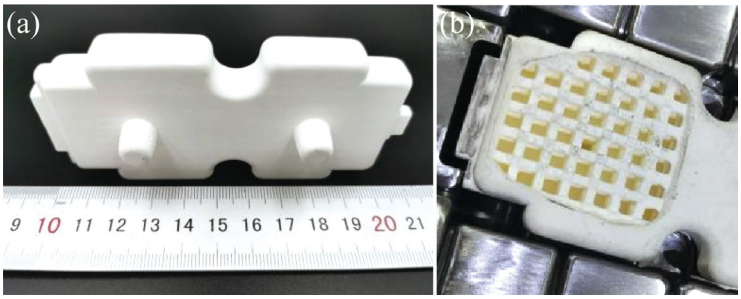

Fig. 12: Sintered sample of the hollow cores: (a) external surface; (b) hollow cavity with lattice structure

The specific dimensions of the hollow cores with lattice structures after compensations were measured to evaluate the dimensional accuracy. The critical dimensions were defined as seen in Fig. 13 covering the width, length, and thickness at different characteristics of the cores. Table 5 presents the comparison between the original design and the data measured from ten samples on these critical dimensions. It can be concluded that the dimensions of the sintered cores are stable and precise, which satisfies the dimensional requirements. However, it should also be noted that the dimensions show positive deviations, suggesting that more precise compensation might be made to further increase the dimensional accuracy.

The sintered cores were also subjected to a series of tests related to the mechanical and thermal properties. Table 6 presents the testing results and the specifications. Due to the difference between the interlayer bonding and bonding within layers, the sintering shrinkage varies in the build direction (Z direction) and the projection plane (X-Y plane). Bending strengths under different conditions were measured including the one reinforced by epoxy resin. The bending strength reaches 11.94 MPa at room temperature and 12.87 MPa at 1,500 °C. The reinforcement of epoxy resin mainly helps strengthen the cores at room temperature to withstand the impact during the wax-injection process. In addition, the creep deformation is 0.345 mm. Compared with the silica-based cores in previous studies as shown in Table 2, the mechanical properties were not much affected due to the hollow design. The qualification of the cores for investment casting was finally verified by the practical casting process.

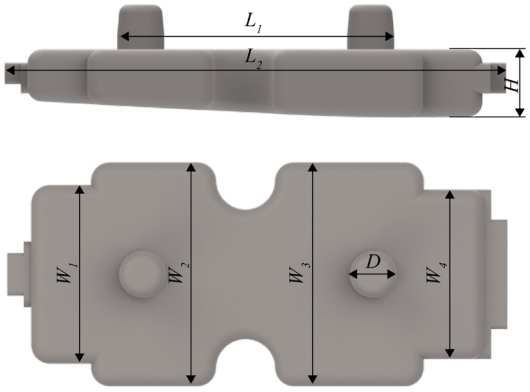

Fig. 13: Specified dimensions of the cores to evaluate the dimensional accuracy

Table 5: Comparison of the sintered ceramic cores and the design on the specified dimensions

Dimensions	Design (mm)	Sintered sample (mm)	Mean error (mm)	Mean relative error (%)
L_1	59.732	59.931 ± 0.197	0.199	0.333
L_2	107.730	107.928 ± 0.113	0.198	0.184
H	14.480	14.447 ± 0.054	−0.033	−0.228
W_1	38.670	38.666 ± 0.085	−0.004	−0.010
W_2	48.440	48.623 ± 0.109	0.183	0.378
W_3	48.440	48.674 ± 0.083	0.234	0.483
W_4	36.636	36.745 ± 0.101	0.109	0.298
D	10.190	10.245 ± 0.072	0.055	0.540

Table 6: Properties of the sintered ceramic core with the corresponding test method

Parameter	Value	Test method
Sintering shrinkage	4.60 % (in the build direction) 3.14 % (in the projection plane)	Specimen size: 6×6×6 mm^3
Apparent porosity Water absorption Bulk density	28.0% 15.6% 1.82 $g·cm^{-3}$	Standard HB 5353.1–2004 Archimedes' method
Bending strength	11.94 MPa (room temperature) 12.87 MPa (1,500 °C) 27.00 MPa (reinforced by epoxy resin)	Standard HB 5353.3–2004 Three-point bending test Span: 30 mm Specimen size: 10×4×40 mm^3
Creep deformation	0.345 mm (1,500 °C, 30 min)	Standard HB 5353.4–2004 Double cantilever beam test Span: 100 mm Specimen size: 2×6×120 mm^3
Thermal expansion coefficient	1.45×10^{-6} K^{-1} (25–1,000 °C)	Standard GB/T 16535–2008 Push-rod test

In addition, the microstructures of the sintered ceramic cores were observed. Figure 14 presents the distribution and sizes of the pores. The pores are dense with uniform sizes, which can promote the removal of the cores without substantially harming the mechanical strength. Furthermore, Fig. 15 presents the EDS characterized element distribution. As Fig. 15(c) shows, zirconium silicate ($ZrSiO_4$) is evenly distributed. Considering that the content of zirconium silicate to fused silica (SiO_2) is 4:14, the even distribution of fused silica can also be concluded from the element distribution of Si in Fig. 15(d). With a 5.3wt.% content, alumina (Al_2O_3) is only partly distributed, but also well mixed with the other contents.

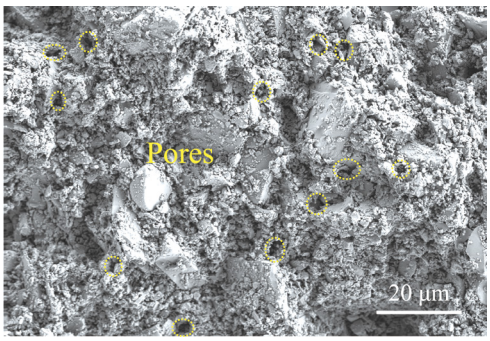

Fig. 14: Microstructure of sintered ceramic core sample showing the distribution of pores

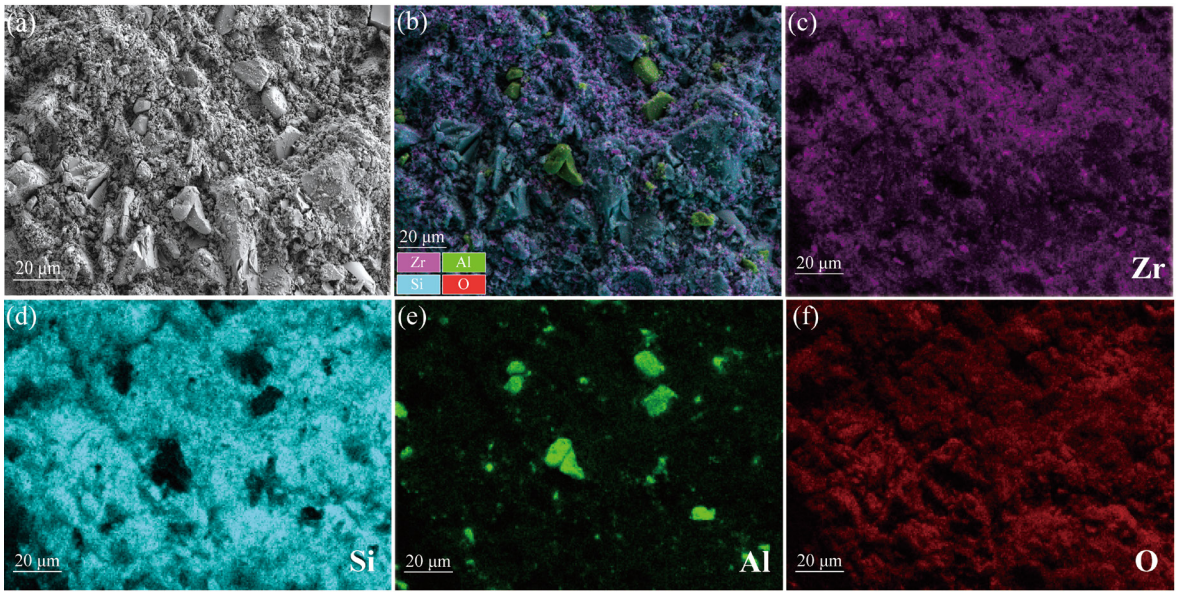

Fig. 15: Microstructure of the sintered ceramic core sample with EDS characterized element distribution: (a) SEM image; (b) EDS image of all the elements; (c) element distribution of Zr; (d) element distribution of Si; (e) element distribution of Al; (f) element distribution of O

3.3 Forming quality of castings

The ceramic cores with the lattice structures show superior performance in terms of both dimensional precision and sintering properties. Practical castings were produced using the cores to verify if they could meet the requirements of the work conditions and obtain high-quality castings. As seen in Fig. 16(a), wax patterns were firstly formed covering the cores. Figure 16(b) presents the X-ray image of the core inside the wax pattern which is completely covered and free of defects. The casting characteristics corresponding to the external shape of the cores are shown in Fig. 16(c).

To further verify the shaping quality of the casting characteristics, the final castings were cut to examine the quality of the cavities, as shown in Fig. 17. The results of the surface roughness (S_a) measurement using an optical profilometer (ZYGO Co., NexView) are also presented. The roughnesses of the cores are mostly below 3 μm while those on the casting surface are controlled within 2 μm. In practical experience, such fine surfaces can hardly be achieved with cores fabricated by traditional methods including injection moulding. In addition, it can be concluded that the surfaces of the castings are smoother than those of the cores. This phenomenon may be attributed to the limitation of the wettability of the metal-ceramic interface. The casting surface does not duplicate some of the details of the core surface that are within several microns. It should also be noted that, for the stereolithography-fabricated cores, the roughnesses at the projection surface (Position 1 and Position 3) are higher than those on the side surface (Position 2). This difference in the cores is also transferred to the castings. Figure 18 presents the microstructures of the two surfaces, which explains the difference. The side surface is at the edges of the layers and therefore scattered powders occur, which can also be attributed to the transition between the irregular edges of different layers caused by light scattering during stereolithography [35]. In contrast, within each layer, the projection surface is much smoother.

During the casting verification, it is also found that the core-removal efficiency is promoted by adopting the lattice structure. Core removal is completed within 10 h with the hollow cores while the solid cores usually take 33 to 36 h. The lattice structure expands the contact area with the solution and reduces the materials to be removed.

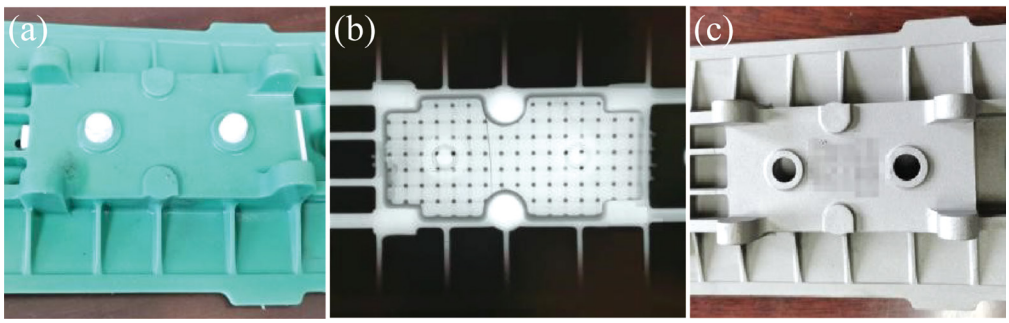

Fig. 16: Usage of the ceramic cores during the practical casting verification: (a) wax pattern with a core inside; (b) X-ray image of the wax pattern with the core inside; (c) casting characteristic corresponding to the core

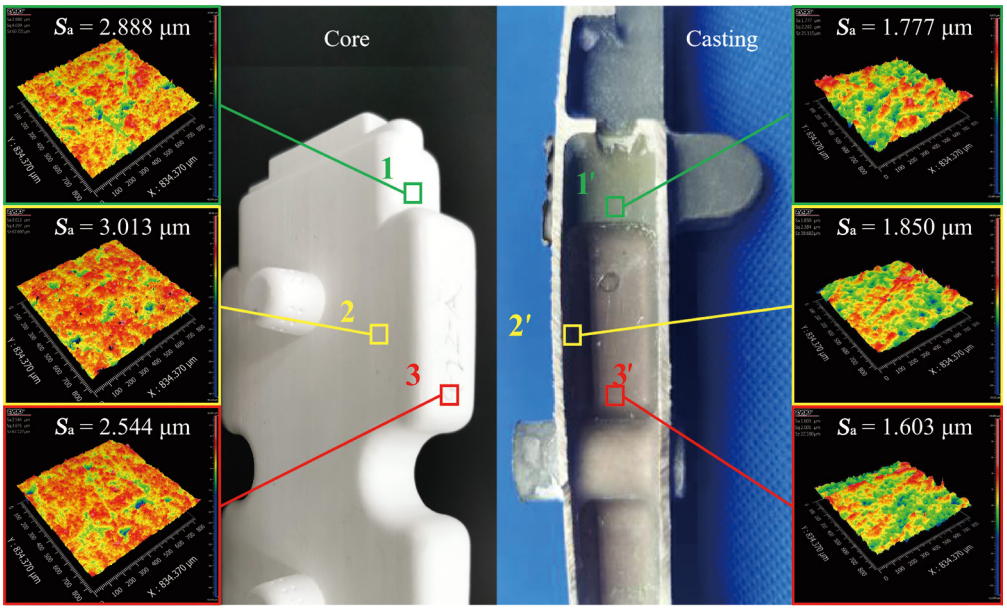

Fig. 17: Results of surface roughness measurement of the core and casting samples. Roughnesses measured at Positions 1 and 3 that lie on the projection surface perpendicular to the build direction are higher than that at Position 2 lying on the side surface. Correspondingly, roughnesses measured at Positions 1' and 3' on the casting are higher than that at Position 2'

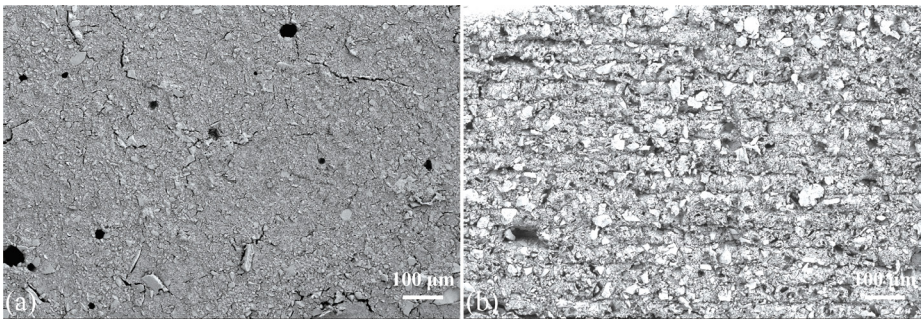

Fig. 18: Microstructures of the sintered core samples: (a) projection surface perpendicular to the build direction; (b) side surface parallel to the build direction

4 Conclusions

Hollow ceramic cores with lattice structures were designed and fabricated using the ceramic stereolithography method to avoid the defects of solid cores while providing sufficient mechanical strength. Following conclusions are obtained:

(1) For green bodies of the cores, high dimensional accuracy can be achieved with compensations for the excess cure width. For the sintered bodies, the hollow design with lattice structures effectively avoids cracks and reduces the dimensional errors led by shrinkage, while does not obviously deteriorate the mechanical performance of the cores. The key dimensions of the cores are controlled within ±0.25 mm. The bending strength reaches 11.94 MPa at room temperature and 12.87 MPa at 1,500 °C with a creep deformation of 0.345 mm.

(2) Casting verifications using the fabricated cores prove that the

hollow cores meet the requirements of investment casting. Smooth casting surfaces are obtained with surface roughness within 2 μm. In addition, the lattice structure also improves the core-removal efficiency by over 3 times.

Acknowledgements

This study was supported by the National Natural Science Foundation of China (Grant No. 52175333); Tribology Science Fund of the State Key Laboratory of Tribology, Tsinghua University (Grant No. SKLT2021B05); Foshan Science and Technology Innovation Team Project (Grant No. 2018IT100142); National Science and Technology Major Project of China (Grant No. J2019-VII-0002-0142).

References

[1] Schmid S K S R. Manufacturing processes for engineering materials. Singapore: Pearson Education, 2008: 225–226.
[2] Wereszczak A A, Breder K, Ferber M K, et al. Dimensional changes and creep of silica core ceramics used in investment casting of superalloys. J. Mater. Sci., 2002, 37(19): 4235–4245.
[3] Gromada M, Świeca A, Kostecki M, et al. Ceramic cores for turbine blades via injection moulding. J. Mater. Process. Technol., 2015, 220: 107–112.
[4] Zhao H P, Ye C S, Fan Z T. 3D printing of calcia-based ceramic core composites. Advances in Science and Technology, 2014, 88: 65–69.
[5] Park H Y, Kim E H, Choi H H, et al. New conversion process for fabricating a ceramic core by a 3D printing technique. Surf. Coat. Technol., 2017, 332: 527–532.
[6] Zhao H P, Ye C S, Fan Z T, et al. 3D printing of cao-based ceramic core using nanozirconia suspension as a binder. J. Eur. Ceram. Soc., 2017, 37(15): 5119–5125.
[7] Tang S Y, Fan Z T, Zhao H P, et al. Layered extrusion forming–a simple and green method for additive manufacturing ceramic core. Int. J. Adv. Manuf. Technol., 2018, 96(9–12): 3809–3819.
[8] Zheng W, Wu J M, Chen S, et al. Fabrication of high-performance silica-based ceramic cores through selective laser sintering combined with vacuum infiltration. Addit. Manuf., 2021, 48: 102396.
[9] Halloran J W. Ceramic stereolithography: Additive manufacturing for ceramics by photopolymerization. Annu. Rev. Mater. Res., 2016, 46(1): 19–40.
[10] Hu K H, Wei Y M, Lu Z G, et al. Design of a shaping system for stereolithography with high solid loading ceramic suspensions. 3D Print. Addit. Manuf., 2018, 5(4): 311–318.
[11] Tang J, Guo X, Chang H Q, et al. The preparation of SiC ceramic photosensitive slurry for rapid stereolithography. J. Eur. Ceram. Soc., 2021, 41(15): 7516–7524.
[12] Ding G J, He R J, Zhang K, et al. Stereolithography 3D printing of SiC ceramic with potential for lightweight optical mirror. Ceram. Int., 2020, 46(11): 18785–18790.
[13] Chen F, Zhu H, Wu J M, et al. Preparation and biological evaluation of ZrO_2 all-ceramic teeth by DLP technology. Ceram. Int., 2020, 46(8): 11268–11274.
[14] Chen Z W, Li Z Y, Li J J, et al. 3D printing of ceramics: A review. J. Eur. Ceram. Soc., 2019, 39(4): 661–687.
[15] Corcione C E, Greco A, Montagna F, et al. Silica moulds built by stereolithography. J. Mater. Sci., 2005, 40(18): 4899–4904.
[16] Halloran J W, Tomeckova V, Gentry S, et al. Photopolymerization of powder suspensions for shaping ceramics. J. Eur. Ceram. Soc., 2011, 31(14): 2613–2619.
[17] Bae C J, Halloran J W. Integrally cored ceramic mold fabricated by ceramic stereolithography. Int. J. Appl. Ceram. Technol., 2011, 8(6): 1255–1262.
[18] Hu K, Lu Z, Lu K, et al. Additive manufacturing of complex ceramic cores and verification of casting process. J. Mech. Eng., 2021, 57(3): 227–234.
[19] Xu X Q, Niu S X, Wang X G, et al. Fabrication and casting simulation of composite ceramic cores with silica nanopowders. Ceram. Int., 2019, 45(15): 19283–19288.
[20] Niu S X, Xu X Q, Li X, et al. Microstructure evolution and properties of silica-based ceramic cores reinforced by mullite fibers. J. Alloys Compd., 2020, 829: 154494.
[21] Li H, Hu K H, Liu Y S, et al. Improved mechanical properties of silica ceramic cores prepared by 3D printing and sintering processes. Scr. Mater., 2021, 194: 113665.
[22] Wang X G, Zhou Y L, Zhou L, et al. Microstructure and properties evolution of silicon-based ceramic cores fabricated by 3D printing with stair-stepping effect control. J. Eur. Ceram. Soc., 2021, 41(8): 4650–4657.
[23] Santoliquido O, Bianchi G, Eggenschwiler P D, et al. Additive manufacturing of periodic ceramic substrates for automotive catalyst supports. Int. J. Appl. Ceram. Technol., 2017, 14(6): 1164–1173.
[24] Mei H, Huang W Z, Zhao Y Z, et al. Strengthening three-dimensional printed ultra-light ceramic lattices. J. Am. Ceram. Soc., 2019, 102(9): 5082–5089.
[25] Shuai X, Zeng Y, Li P, et al. Fabrication of fine and complex lattice structure Al_2O_3 ceramic by digital light processing 3D printing technology. J. Mater. Sci., 2020, 55(16): 6771–6782.
[26] Markandan K, Lai C Q. Enhanced mechanical properties of 3D printed graphene-polymer composite lattices at very low graphene concentrations. Composites, Part A: Applied Science and Manufacturing, 2020, 129: 105726.
[27] Zheng X, Lee H, Weisgraber T H, et al. Ultralight, ultrastiff mechanical metamaterials. Sci., 2014, 344(6190): 1373–1377.
[28] Xu S Q, Shen J H, Zhou S W, et al. Design of lattice structures with controlled anisotropy. Mater. Des., 2016, 93: 443–447.
[29] Yap X Y, Seetoh I, Goh W L, et al. Mechanical properties and failure behaviour of architected alumina microlattices fabricated by stereolithography 3D printing. Int. J. Mech. Sci., 2021, 196: 106285.
[30] Qian C, Li X, Hu K, et al. Thermal behaviour in the stereolithography process for Al_2O_3 ceramic suspension. Key Eng. Mater., 2021, 871: 189–202.
[31] Bae C J, Halloran J W. Influence of residual monomer on cracking in ceramics fabricated by stereolithography. Int. J. Appl. Ceram. Technol., 2011, 8(6): 1289–1295.
[32] Santoliquido O, Camerota F, Ortona A. The influence of topology on dlp 3D printing, debinding and sintering of ceramic periodic architectures designed to replace bulky components. Open Ceram., 2021, 5: 100059.
[33] Gentry S P, Halloran J W. Depth and width of cured lines in photopolymerizable ceramic suspensions. J. Eur. Ceram. Soc., 2013, 33(10): 1981–1988.
[34] Mitteramskogler G, Gmeiner R, Felzmann R, et al. Light curing strategies for lithography-based additive manufacturing of customized ceramics. Addit. Manuf., 2014, 1–4: 110–118.
[35] Qian C C, Hu K H, Li J H, et al. The effect of light scattering in stereolithography ceramic manufacturing. J. Eur. Ceram. Soc., 2021, 41(14): 7141–7154.